

# Terahertz Switch Based on Waveguide-Cavity-Waveguide Comprising Cylindrical Spoof Surface Plasmon Polariton

Mahdi Aghadjani and Pinaki Mazumder, *Fellow, IEEE*

**Abstract**—This paper demonstrates a terahertz (THz) switch that comprises a metallic perfect conductor in the form of periodically corrugated cylindrical waveguides surrounding a dielectric medium consisting of GaAs compound semiconductor. The proposed switch deploys a composite waveguide-cavity-waveguide structure. The switch controls its state by dynamically altering the optical properties of an engineered nonlinear material inside the cavity, while the corrugated waveguides on both sides of the cavity are incorporated to limit the propagation of electromagnetic (EM) waves at nearly THz frequencies only. At the resonant frequency, the corrugated waveguide allows strong EM confinement inside the grooves. The cavity has been designed to achieve a high quality factor as well as to trap EM waves for a significant period of time. Small changes in the GaAs refractive index inside the grooves can alter the cavity resonant frequency. Localized doping near the metal conductor inside the cavity is implemented so that by applying a voltage between the metal electrode and the depletion region in the dielectric medium, the switch can be altered from the ON state to the OFF state, and vice versa.

**Index Terms**—Free carrier concentration, spoof surface plasmon polariton (SSPP), terahertz (THz), waveguide-cavity-waveguide (WCW).

## I. INTRODUCTION

THERE is significant interest in devices that work in frequency ranges from 0.3 to 10 THz. Such devices find applications in areas such as imaging, spectroscopy, biomedical sensing, ultrafast computer circuits, astronomical remote sensing, and hazardous chemical detection [1]–[10]. The confinement and concentration of terahertz (THz) radiation in small volumes of subwavelength structures can be utilized to control the transmission of electromagnetic (EM) waves by enhancing interactions between the EM waves and nonlinear materials [11], [12]. The strong mode of confinement is achieved in this paper by confining the spoof surface plasmon polariton (SSPP) waves to periodically corrugated metallic structures [13]–[18]. This newly developed method can overcome the group velocity dispersion of THz waves and

weak guiding at THz frequencies. The SSPP modes exhibit features such as field enhancement and localization. In this technique, the transverse mode of SSPP mimics the behavior of surface plasmon polariton at the metal–dielectric interface in metallic wires [14]. The SSPP structures have multiple passbands and stopbands. These bands can be engineered by changing the geometric dimensions and materials inside the structures. The proposed switch is inspired by [14] and [15].

THz generation and detection methods have been around for many years, but generally THz systems have not succeeded in making commercial inroads until very recently [19]. The progress in THz engineering has been stymied due to the lack of ability to control and manipulate THz signals. Unlike charge-based field-effect and potential-effect devices, both photonic and THz three-terminal switches are difficult to build because of lack of controllability of THz waves either optically or magnetically, especially within the confines of device geometries. Metamaterial, liquid crystal (LC), and nonlinear Kerr materials are potentially suitable for devising the control of EM waves, as they can be manipulated for absorption as well as resonance in the THz range. However, there are still some challenges that need to be resolved before those devices can be used in THz digital logic. For example, distributed voltage needs to be applied along the LC to make it uniformly polarized. Also, the switching speed of LCs is significantly low. The metamaterial structures are comparably big with respect to the LC structure and they work in free space communications. Kerr materials need to be pumped by optical signals to tune their loss or refractive index. This requires mostly high-power optical pumping.

To overcome the above-mentioned difficulties in deploying LCs and Kerr materials, semiconductors (Si, InSb) can be used [20]–[22] so that by free carrier injection through a p-i-n junction, the transmittance (or coupling efficiency) of their proposed structures in THz frequencies can be controlled. Due to the large imaginary part of Si permittivity in the THz range, such design can only be effectively used up to near-infrared frequencies.

In this paper, we propose a new THz switch comprising a cylindrical SSPP (C-SSPP) structure. We demonstrate that the C-SSPP has strong mode confinement, discrete transmission bands, and high quality factor in THz domain. The proposed switch works based on waveguide-cavity-waveguide (WCW) structure. The cavity is connected to identical corrugated cylindrical waveguides in both sides. The new structure can work as an active switch or modulator.

Manuscript received October 13, 2014; revised December 6, 2014 and January 19, 2015; accepted January 22, 2015. Date of current version March 20, 2015. This work was supported in part by the Air Force Office of Scientific Research, Arlington, VA, USA, under Grant FA 9550-12-1-0402, and in part by the National Science Foundation under Grant 1116040. The review of this paper was arranged by Editor M. Thumm.

The authors are with the Department of Electrical Engineering and Computer Science, University of Michigan, Ann Arbor, MI 48109 USA (e-mail: mahdia@umich.edu; pinakimazum@gmail.com).

Color versions of one or more of the figures in this paper are available online at <http://ieeexplore.ieee.org>.

Digital Object Identifier 10.1109/TED.2015.2404783

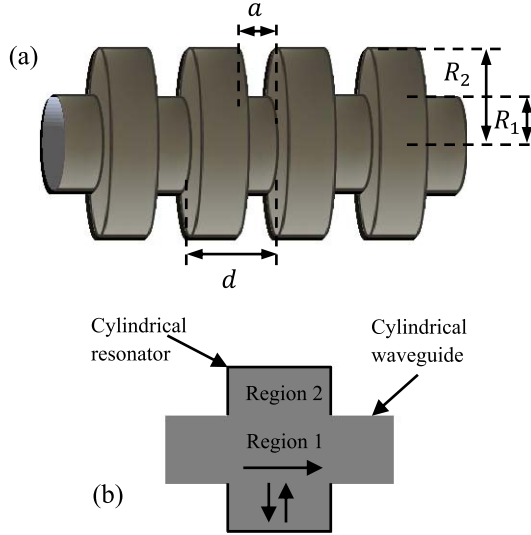


Fig. 1. (a) Schematic of the corrugated cylindrical waveguide with different dimensions labeled. (b) Cross section of unit cell of the structure. The structure can be divided into two sections as shown in the sketch.

Furthermore, the high quality factor cavity and small effective area enable the device to function at the small refractive index modulation ( $\delta n_d/n_d$ ) induced by applying voltage to the metal electrode connections.

This paper is organized as follows. In Section II, a mathematical analysis of the C-SSPP is briefly described. In Section III, we investigate the WCW structure, and in Section IV, the depletion mode is studied to propose the final design.

## II. THEORETICAL ANALYSIS

Fig. 1 shows the overall view of the C-SSPP waveguide and the unit cell of the structure. As can be seen, one period of the waveguide has been divided into two regions. Region 1 acts as a cylindrical waveguide, while Region 2 is a cylindrical resonator. To calculate the dispersion relationship, vectorial EM fields need to be expressed in both Regions 1 and 2. Using rigorous mathematical analysis, the dispersion diagram can be obtained using (1).

In our calculations,  $d$  is the period of the grooves,  $a$  and  $R_2$  stand for the width and radius of the grooves, respectively, while  $R_1$  is the radius of the smooth part of the waveguide.  $n_d$  represents the dielectric index inside the waveguide. Based on Maxwell's equations, mathematical expressions of the TM-polarized and TE-polarized waves propagating in the  $z$ -direction along the grooves can be explicitly written out for both Regions 1 and 2. By satisfying the boundary conditions for tangential fields at the interface of Regions 1 and 2, the dispersion relation of the C-SSPP can be derived using (1). It can be concluded from (1) that the dispersion diagram is a function of the refractive index. Then, by modulating the  $n_d$  with external stimuli, the dispersion diagram can be alerted. The additional variables in (1) are defined as

$$k_\rho^2 + k_z^{m2} = n_d^2 k_0^2, \quad C_m = \sqrt{\frac{a}{d}} \text{sinc}\left(\frac{k_z^m a}{2\pi}\right)$$

$$k_{\rho 2}^2 + \left(\frac{n\pi}{a}\right)^2 = n_d^2 k_0^2$$

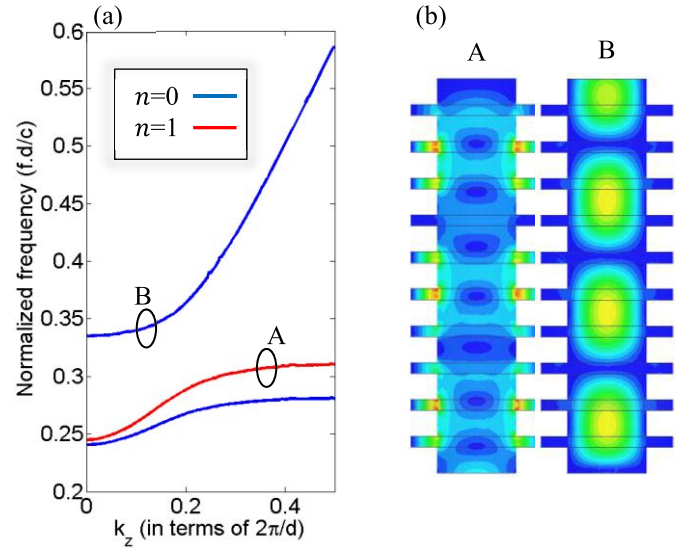


Fig. 2. (a) Dispersion diagram of C-SSPP with the dimensions  $R_1 = 120 \mu\text{m}$ ,  $R_2 = 200 \mu\text{m}$ ,  $d = 100 \mu\text{m}$ , and  $a = 30 \mu\text{m}$ . (b) Electric field magnitude inside the smooth part of the waveguide and grooves at two different frequencies.

where  $k_z^m$  denotes the wavevector of  $m^{\text{th}}$ -order Bloch-Floquet mode along the  $z$ -axis

$$\begin{bmatrix} \sum_{m=-M}^M A_m k_\rho \frac{I'_n(k_\rho R_1)}{I_n(k_\rho R_1)} + 1 & \sum_{m=-M}^M \frac{N B_m C_m}{A R_1} I'_n(k_\rho R_1) \\ \sum_{m=-M}^M \frac{A_m C_m k_\rho}{B \omega R_1} N k_z I_n(k_\rho R_1) & \sum_{m=-M}^M \frac{B_m C_m k_\rho I'_n(k_\rho R_1)}{k_{\rho 2} \frac{2a}{\pi}} - 1 \end{bmatrix} \times \begin{bmatrix} A^+ \\ B^+ \end{bmatrix} = \begin{bmatrix} 0 \\ 0 \end{bmatrix}. \quad (1)$$

In which

$$A_m = \frac{-k_{\rho 2}}{k_\rho} \frac{(H_n^1(k_{\rho 2} R_2) H_n^2(k_{\rho 2} R_1) - H_n^2(k_{\rho 2} R_2) H_n^1(k_{\rho 2} R_1))}{(H_n^1(k_{\rho 2} R_2) H_n^{2'}(k_{\rho 2} R_1) - H_n^2(k_{\rho 2} R_2) H_n^{1'}(k_{\rho 2} R_1))} C_m^2$$

$$B_m = \frac{k_{\rho 2}}{k_\rho} \frac{(H_n^1(k_{\rho 2} R_2) H_n^{2'}(k_{\rho 2} R_1) - H_n^2(k_{\rho 2} R_2) H_n^{1'}(k_{\rho 2} R_1))}{(H_n^1(k_{\rho 2} R_2) H_n^2(k_{\rho 2} R_1) - H_n^2(k_{\rho 2} R_2) H_n^1(k_{\rho 2} R_1))} C_m^2$$

$$A = H_n^1(k_{\rho 2} R_2) H_n^2(k_{\rho 2} R_1) - H_n^2(k_{\rho 2} R_2) H_n^1(k_{\rho 2} R_1)$$

$$B = H_n^1(k_{\rho 2} R_2) H_n^{2'}(k_{\rho 2} R_1) - H_n^2(k_{\rho 2} R_2) H_n^{1'}(k_{\rho 2} R_1) \quad (2)$$

where  $H_n^{1,2}(k_{\rho 2} \rho)$  are Hankel functions of the first and second kind and  $I_n(k_\rho \rho)$  is the modified Bessel function of the first kind. Fig. 2(a) shows the dispersion diagram for  $n = 0$  and  $n = 1$ , and Fig. 2(b) shows the electric field inside the C-SSPP waveguide at two different frequencies. When the operating frequency is in the vicinity of the bandgap [point A in Fig. 2(a)], it shows strong mode confinement inside the grooves and slow wave propagation along the structure. Increasing the operating frequency over the band edge [point B in Fig. 2(a)], localization decreases and the SSPP mode no longer exists. The localization of SSPP modes inside the structure helps us to alter the dispersion characteristics by inserting small changes in the refractive

TABLE I  
VARIABLES IN MODIFIED DRUDE DIELECTRIC CONSTANT MODEL

$\epsilon_0$	Vacuum permittivity
$\epsilon_s$	Static dielectric constant
$E$	Electron charge
$\omega_{LO}$	Longitudinal optical phonon resonance
$\omega_{TO}$	Transverse optical phonon resonance
$\Gamma$	Free carrier coherent decay factor
$m_e$	Electron effective mass
$\gamma$	Phonon damping constant
$N$	Free carrier density

index inside the grooves instead of changing it in the whole structure.

In the following sections, the localization of SSPP modes is used to enhance the effect of refractive index change in the transmission characteristics of the C-SSPP.

### III. DESIGN OF THE THz WAVEGUIDE-CAVITY-WAVEGUIDE SWITCH

In this section, we investigate the WCW structure for THz switches and the mechanism to control the flow of EM fields inside the structure.

The dielectric constant of a semiconductor can be described as a function of frequency using the Drude model [23], [24]

$$\epsilon(\omega) = \epsilon_\infty - \frac{\omega_p^2}{\omega(\omega + i\Gamma)}. \quad (3)$$

In which

$$\omega_p = \sqrt{\frac{Ne^2}{m_e \epsilon_\infty \epsilon_0}} \quad (4)$$

$$\epsilon_\infty = \epsilon_s \left( \frac{\omega_{TO}}{\omega_{LO}} \right)^2.$$

To implement the optical phonon vibrations of crystal lattice in heteropolar semiconductor at higher frequency, the Drude model needs some modifications. For the heteropolar semiconductors, the split of transverse and longitudinal phonon energies at zero momentum give rise to an extra term in the permittivity calculation formula. The modified Drude model can be described as

$$\epsilon(\omega) = \epsilon_\infty \left( 1 + \frac{\omega_{LO}^2 - \omega_{TO}^2}{\omega_{TO}^2 - \omega^2 - i\omega\gamma} - \frac{\omega_p^2}{\omega(\omega + i\Gamma)} \right). \quad (5)$$

The variables in (5) are explained in Table I. Using (5), the dielectric constant of GaAs is calculated versus frequency in Fig. 3(a). The effect of phonon resonances can be observed by the sharp peak in the imaginary part of permittivity. Fig. 3(b) shows the real and imaginary parts of the dielectric constant as functions of carrier density ( $N$ ) in semiconductor at a frequency of 10.5 THz.

The Kramers–Kronig relationship dictates coupled evolution of the real and imaginary parts of the dielectric constant. Then a change in absorption must be accompanied by the shift in phase accumulation or real part. In Fig. 3(b), it is shown that

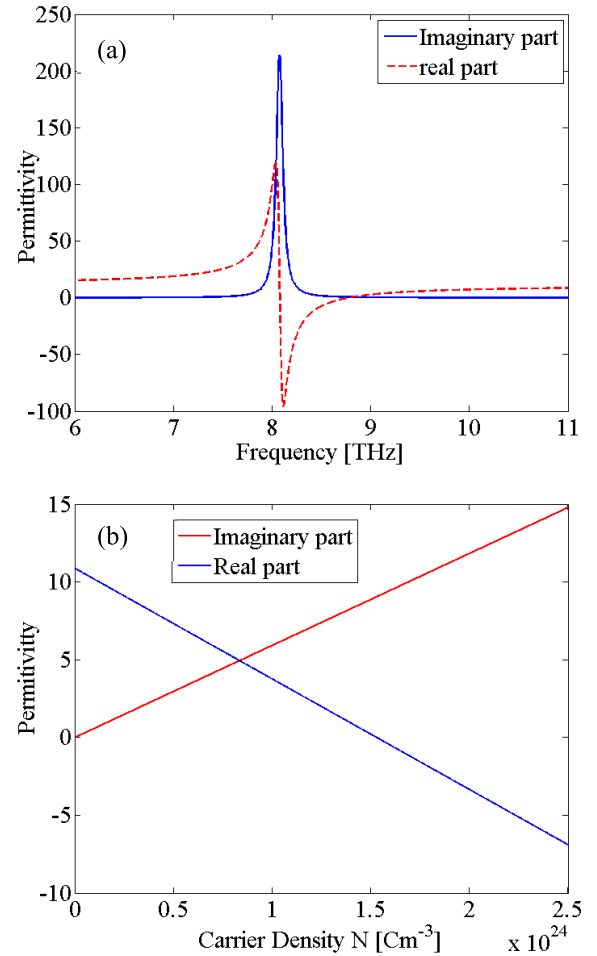


Fig. 3. (a) Real and imaginary parts of GaAs permittivity as functions of frequency for free carrier density of  $N = 2 \times 10^6 \text{ cm}^{-3}$ . (b) Real and imaginary parts of permittivity as functions of free carrier density at a frequency of 10 THz.

by increasing the carrier density, the real part decreases and the imaginary part increases. In other words, higher carrier density results in higher loss. In this paper, the carrier density for the doped region is set to be  $N = 2 \times 10^{17} \text{ cm}^{-3}$  and the corresponding permittivity is  $16.69 + i4.67$ . As can be observed in Fig. 3(a), there is an abrupt change in the real part of permittivity around 8.0 THz. Our operational frequency is set around 10.5 THz where the real and imaginary parts of permittivity show milder change versus frequency. The calculated permittivity at 10.5 THz is  $8.01 + i0.05$ . There are other materials that can be used as a substitution for GaAs, such as InSb or Si. However, GaAs is preferable because of its low intrinsic free carrier density and higher carrier mobility compared with other mentioned choices.

Enhancement and depletion modes are known as a working mode based on injection and depletion of free carriers in the doped semiconductor. These two modes are being used in this section and the following section to describe the THz switch states.

Here, we focus on the WCW structure with potential application as THz switch or filter. Fig. 4(a) shows the schematic view of our proposed WCW THz switch, consisting

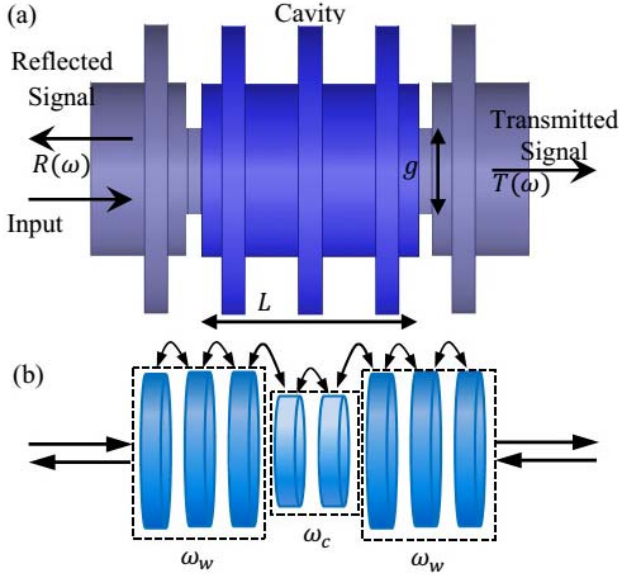


Fig. 4. (a) Schematic of the THz WCW structure. (b) THz waveguide and cavity can be assumed as an equally spaced cylindrical resonator array. The coupling frequencies for waveguide and cavity resonators are  $\omega_w$  and  $\omega_c$ , respectively.

of two parts: 1) cavity and 2) waveguide. The waveguide can be assumed as equally spaced cylindrical resonators, which are placed along the cylindrical waveguide. Fig. 4(b) shows the wave propagation mechanism in the WCW structure. As shown, the structure can be regarded as equally spaced resonator array. The resonators in the waveguide are coupled at  $\omega_w$  and the coupled frequency for the cavity's resonators is  $\omega_c$ . When the resonant frequencies of both parts are the same, the EM wave can couple from the waveguide to cavity and vice versa. Then to obtain the highest transmission in the switch, it is essential that  $\omega_w$  and  $\omega_c$  coincide. In the next paragraph we use a mathematical model to describe the power transmission in the proposed structure, and then we investigate the parameters that are taking effect in the power transmission characteristic.

Using temporal coupled-wave analysis, the transmission and the reflection of waveguide-cavity can be described as [26], [27]

$$T(\omega) = \frac{\Gamma_c^2}{(\omega - \omega_w)^2 + \Gamma_c^2} \quad (6)$$

$$R(\omega) = \frac{(\omega - \omega_w)^2}{(\omega - \omega_w)^2 + \Gamma_c^2}. \quad (7)$$

And  $\Gamma_c$  can be described using

$$\Gamma_c = \frac{\omega_c}{2Q}. \quad (8)$$

In (6) and (7), the cavity decay rate ( $\Gamma_0$ ) is assumed to be smaller than the cavity coupling ratio ( $\Gamma_c$ ). This assumption is acceptable in our case as the loss is very small. The  $\omega_c$  is the resonant frequency of the cavity that can be controlled by changing the groove's height or altering the refractive index inside the dielectric. The groove's height is predetermined and cannot be changed after design so the only option to tune the

resonant frequency is changing the refractive index. In this design, when there are no stimuli and the operating frequency is far from the cavity's resonant frequency compared with  $\Gamma_c$ , ( $|\omega - \omega_c| \gg \Gamma_c$ ), all the power reflects back and the switch is in the OFF-state. When the operation frequency is close to the cavity's resonant frequency ( $|\omega - \omega_c| \ll \Gamma_c$ ), the transmission in (6) is approximately 1 and the switch is in the ON-state.

To introduce the parameters that can enhance the switching ratio, we approximate (8) as

$$\Gamma_c \sim \frac{(1-R)v_g}{L_{cav}}. \quad (9)$$

The  $\Gamma_c$  is described as a function of reflective coefficient  $R$  and group velocity  $v_g$ . Based on (6) and (7), to enhance the switching ratio, we need to increase the reflective coefficient and decrease group velocity by employing slow waves. Then to achieve the high switching ratio, two main parameters of the cavity should be considered: the quality factor that is inversely proportional to cavity decay rate in (7) and the effective volume  $V_{eff}$  that controls the cavity's photon intensity [25].

The proposed C-SSPP structure can support the slow waves that have a small group velocity. Additionally, the cavity can trap EM waves for a significant period of time, resulting in a high quality factor. Then based on what was discussed in the previous paragraph, this structure can have a high switching ratio.

In our design, the cavity and waveguides portions are identical, but they are separated from the waveguide through inserting a circular iris between the waveguides and the cavity. As shown in Fig. 2(a), if there is no iris between the cavity and waveguides, the structure acts like a band reject filter. However, by inserting the iris between the waveguide and the cavity, it acts as a band pass filter. By changing the iris radius, we can adjust the passing bandwidth. In other words, inserting the iris and changing its radius alter the effective volume and, as a result, the quality factor and the cavity's bandwidth change. The simulations show that by decreasing the iris radius, the bandwidth is also reduced. It is noteworthy that the relative bandwidth in the switch with a longer cavity lengths is bigger due to the higher loss. The iris radius for both cases in Fig. 5 is set to be  $R_1/1.5$  and the iris length is set to be  $a/4$ . In the next section, the depletion mode is used to alter the resonant frequency of the cavity.

As mentioned earlier and shown in Fig. 2(a), to have the SSPP mode propagating along the structure, the operating frequency must be around 0.5 THz, but to use the GaAs properties in our structure, the operating frequency should be 10.5 THz. By scaling the C-SSPP structure in Fig. 2(b), the new dimensions are: 1)  $R_1 = 3.8 \mu\text{m}$ ; 2)  $R_2 = 6.34 \mu\text{m}$ ; 3)  $d = 3.7 \mu\text{m}$ ; and 4)  $a = 2.2 \mu\text{m}$ . Fig. 5 shows the power transmission of the switch versus frequency for two different cavity lengths. As depicted, both structures are acting as a band pass filter with a high quality factor. In the longer cavity length, the EM wave experiences higher loss as the wave and material interaction is higher, and as a result, the maximum transmission is lower compared with the smaller cavity length.

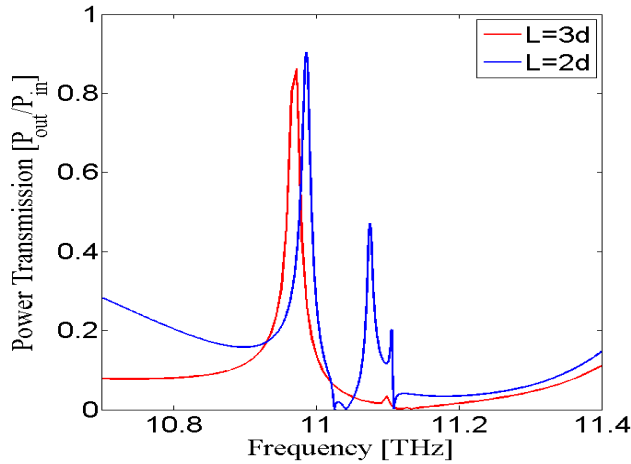


Fig. 5. Power transmission for the bandpass filter at different frequencies for two different cavity lengths. The blue curve represents THz switch with two resonators in the cavity and the red curve shows the power transmission for cavity with three resonators. The dimensions are:  $R_1 = 3.8 \mu\text{m}$ ,  $R_2 = 6.34 \mu\text{m}$ ,  $d = 3.7 \mu\text{m}$ , and  $a = 2.2 \mu\text{m}$ .

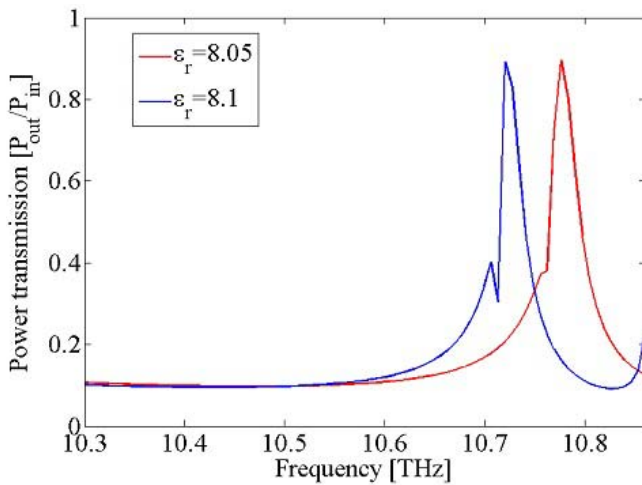


Fig. 6. Power transmission versus frequency for different values of GaAs permittivity.

#### IV. DEPLETION MODE

As explained in Section III, by tuning the waveguide-cavity coupling ratio, the power transmission can be adjusted. Based on (8), the  $\Gamma_c$  is a function of the cavity resonant frequency. Utilizing the depletion mode to change the dielectric refractive index inside the cavity, the resonant frequency can be altered. As the cavity quality factor is high, the small change in refractive index can change the resonance frequency such that the WCW switches from one state to another state.

Fig. 6 shows the power transmission for two different refractive indices inside the cavity. In this plot, the GaAs refractive index is assumed to be constant over the entire cavity. The cavity length is set to be three periods to increase the interaction of EM waves with the refractive index inside the cavity. By changing the real part of permittivity from 8.05 to 8.1, the resonant frequency shifts from 10.78 to 10.72 THz. In principle, as permittivity increases, the resonant frequency of the cavity shifts to lower frequencies. Likewise, when the permittivity decreases, the resonant frequency shifts to higher frequencies.

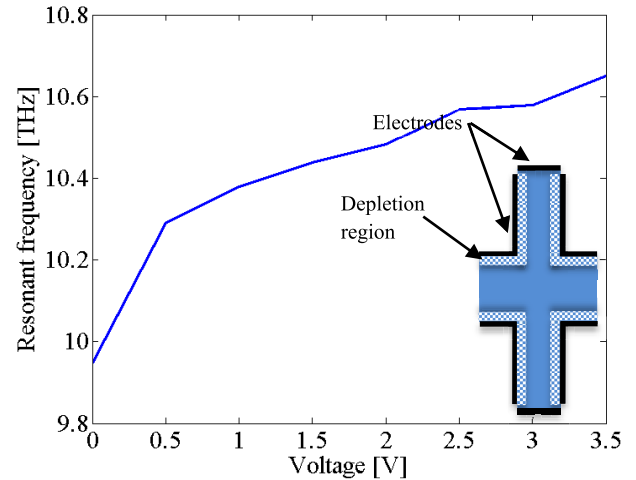


Fig. 7. Resonant frequency of a cavity versus the applied voltage across the metal contact. Inset: connection of the electrodes to the cavity.

Due to technological constraints, it is not practical to alter the refractive index value in the entire cavity. As mentioned earlier, by setting the operating frequency near the groove's resonant frequency, most of the EM power concentrates inside the grooves. Then by changing the refractive index in a portion of the groove's cavity, it is possible to control the flow of EM waves.

In the final design, the free carrier concentration of GaAs inside the groove's cavity is set to  $N = 2 \times 10^{16} \text{ Cm}^{-3}$ . Since the doping concentration is higher than its intrinsic carrier density ( $N = 2 \times 10^6 \text{ Cm}^{-3}$ ), we can utilize the depletion mode in our structure. Where the metal electrode in the cylindrical resonator and the GaAs dielectric contact, a Schottky contact is formed. By applying a voltage to the electrodes, the depletion zone below the metals will appear. The depletion thickness can be calculated using [24]

$$D_{\text{depletion}} = \sqrt{\frac{2\epsilon_s\epsilon_0(V_{\text{bi}} + V)}{eN}}. \quad (10)$$

Here,  $V$  is the applied voltage to the patches and  $V_{\text{bi}}$  is the built-in voltage of the semiconductor metal junction. Other variables are described in Table I. For the GaAs-metal junction, the  $V_{\text{bi}} = 0.75 \text{ V}$ . By changing the voltage across the electrodes, the depletion depth will be formed and the effective permittivity of GaAs can be tuned. The switch state can alter from ON to OFF and vice versa by controlling the depletion region in a layer of GaAs that is thin relative to the groove's width. Fig. 7 shows the resonant frequency versus different voltages. The permittivity of the depletion region can be calculated setting  $N = 0$  in (4). This results in  $\epsilon = 8.051 + i0.05$ , which is close to the intrinsic value of permittivity with  $N = 2 \times 10^6 \text{ Cm}^{-3}$ . By increasing the voltage, the depth of the depletion region increases, which leads to a decrease in the effective permittivity of the dielectric inside the cavity. As mentioned earlier, decrease in permittivity will shift the resonant frequency to the higher side.

Fig. 8 shows the power transmission for two different voltages across the metal contacts and the electric field magnitude at two different frequencies when the voltage is set to 2 V. As shown in Fig. 8(b), when the operating frequency

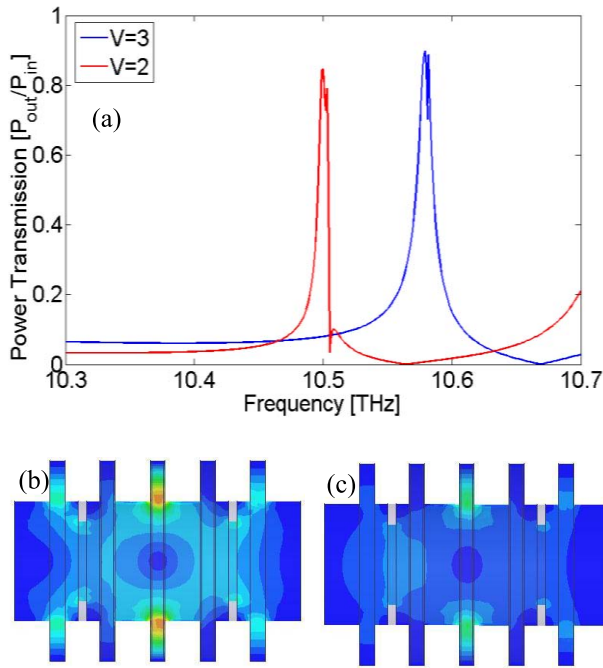


Fig. 8. (a) Power transmission at two different voltages. (b) Electric field magnitude at 10.58 THz. (c) Electric field magnitude at 10.59 THz.

is at 10.58 THz, the power transmission has its maximum value and the electric field concentration is maximum inside the grooves. By increasing or decreasing the frequency from 10.58 THz the power transmission is reduced. Fig. 8(c) shows the electric field magnitude at 10.59 THz. As can be seen, the electric fields are weaker in the cavity.

## V. CONCLUSION

In this paper, propagation of SSPP along a periodically corrugated cylindrical waveguide has been investigated. It has been demonstrated that the propagation of SSPP signals can be controlled by modulating the refractive index of the dielectric material. At resonant frequency, it supports strong EM confinement inside the resonating grooves. The cavity has a high quality factor. Small changes in dielectric inside the cavity can change the resonant frequency. It is shown that by implementing localized doping near the metal conductor inside the cavities, by applying voltage to the metal electrode, and by depleting the free charges in the dielectric directly underneath the contact, the structure can switch between the ON-state and the OFF-state. The proposed switch can be used in implementing THz Boolean gates. Also, the WCW structure can be utilized to design the Mach-Zehnder interferometer [6], multiplexers, and demultiplexers in biosensing architectures [28].

## REFERENCES

- [1] R. Köhler *et al.*, "Terahertz semiconductor-heterostructure laser," *Nature*, vol. 417, pp. 156–159, May 2002.
- [2] R. Mendis and D. Grischkowsky, "Plastic ribbon THz waveguides," *J. Appl. Phys.*, vol. 88, no. 7, pp. 4449–4451, 2000.
- [3] W. Zhu, A. Agrawal, and A. Nahata, "Planar plasmonic terahertz guided-wave devices," *Opt. Exp.*, vol. 16, no. 9, pp. 6216–6226, 2008.

- [4] D. M. Mittleman, R. H. Jacobsen, and M. C. Nuss, "T-ray imaging," *IEEE J. Sel. Topics Quantum Electron.*, vol. 2, no. 3, pp. 679–692, Sep. 1996.
- [5] P. H. Siegel, "Terahertz technology," *IEEE Trans. Microw. Theory Techn.*, vol. 50, no. 3, pp. 910–928, Mar. 2002.
- [6] Z. Xu and P. Mazumder, "Bio-sensing by Mach-Zehnder interferometer comprising doubly-corrugated spoofed surface plasmon polariton (DC-SSPP) waveguide," *IEEE Trans. Terahertz Sci. Technol.*, vol. 2, no. 4, pp. 460–466, Jul. 2012.
- [7] G. Kumar, A. Cui, S. Pandey, and A. Nahata, "Planar terahertz waveguides based on complementary split ring resonators," *Opt. Exp.*, vol. 19, no. 2, pp. 1072–1080, 2011.
- [8] K. Song and P. Mazumder, "Active terahertz spoof surface plasmon polariton switch comprising the perfect conductor metamaterial," *IEEE Trans. Electron Devices*, vol. 56, no. 11, pp. 2792–2799, Nov. 2009.
- [9] K. Song and P. Mazumder, "Dynamic terahertz spoof surface plasmon-polariton switch based on resonance and absorption," *IEEE Trans. Electron Devices*, vol. 58, no. 7, pp. 2172–2176, Jul. 2011.
- [10] N. Zheng, M. Aghadjani, K. Song, and P. Mazumder, "Metamaterial sensor platforms for terahertz DNA sensing," in *Proc. 13th IEEE Conf. Nanotechnol. (IEEE-NANO)*, Aug. 2013, pp. 315–320.
- [11] J. Dintinger, I. Robel, P. V. Kamat, C. Genet, and T. W. Ebbesen, "Terahertz all-optical molecule-plasmon modulation," *Adv. Mater.*, vol. 18, no. 13, pp. 1645–1648, Jul. 2006.
- [12] J. G. Rivas, J. A. Sánchez, M. Kuttge, P. H. Bolivar, and H. Kurz, "Optically switchable mirrors for surface plasmon polaritons propagating on semiconductor surfaces," *Phys. Rev. B*, vol. 74, no. 24, p. 245324, Dec. 2006.
- [13] F. J. Garcia-Vidal, L. Martín-Moreno, T. W. Ebbesen, and L. Kuipers, "Light passing through subwavelength apertures," *Rev. Modern Phys.*, vol. 82, no. 1, pp. 729–787, Mar. 2010.
- [14] K. Wang and D. M. Mittleman, "Metal wires for terahertz wave guiding," *Nature*, vol. 432, pp. 376–379, Nov. 2004.
- [15] J. B. Pendry, L. Martín-Moreno, and F. J. Garcia-Vidal, "Mimicking surface plasmons with structured surfaces," *Science*, vol. 305, no. 5685, pp. 847–848, Aug. 2004.
- [16] C. R. Williams *et al.*, "Highly confined guiding of terahertz surface plasmon polaritons on structured metal surfaces," *Nature Photon.*, vol. 3, pp. 175–179, Feb. 2008.
- [17] A. I. Fernández-Domínguez, L. Martín-Moreno, F. J. García-Vidal, S. R. Andrews, and S. A. Maier, "Spoof surface plasmon polariton modes propagating along periodically corrugated wires," *IEEE J. Sel. Topics Quantum Electron.*, vol. 14, no. 6, pp. 1515–1521, Nov./Dec. 2008.
- [18] Z. Xu, K. Song, and P. Mazumder, "Analysis of doubly corrugated spoof surface plasmon polariton (DC-SSPP) structure with sub-wavelength transmission at THz frequencies," *IEEE Trans. Terahertz Sci. Technol.*, vol. 2, no. 3, pp. 345–354, May 2012.
- [19] Y. Yuan, J. He, J. Liu, and J. Yao, "Electrically controlled broadband THz switch based on liquid-crystal-filled multi-layer metallic grating structures," *J. Phys., Conf. Ser.*, vol. 276, no. 1, p. 012228, 2011.
- [20] T. A. Ibrahim *et al.*, "Lightwave switching in semiconductor microring devices by free carrier injection," *J. Lightw. Technol.*, vol. 21, no. 12, pp. 2997–3003, Dec. 2003.
- [21] Q. Xu, B. Schmidt, S. Pradhan, and M. Lipson, "Micrometre-scale silicon electro-optic modulator," *Nature*, vol. 435, pp. 325–327, May 2005.
- [22] Q. Xu, S. Manipatruni, B. Schmidt, J. Shakya, and M. Lipson, "12.5 Gbit/s carrier-injection-based silicon micro-ring silicon modulators," *Opt. Exp.*, vol. 15, no. 2, pp. 430–436, 2007.
- [23] S. Adachi, *Optical Properties of Crystalline and Amorphous Semiconductors: Materials and Fundamental Principles*. Norwell, MA, USA: Kluwer, 1999.
- [24] M. S. Shur, *Introduction to Electronic Devices*. New York, NY, USA: Wiley, 1996.
- [25] K. J. Vahala, "Optical microcavities," *Nature*, vol. 424, no. 6950, pp. 839–846, Aug. 2003.
- [26] W. Suh, Z. Wang, and S. Fan, "Temporal coupled-mode theory and the presence of non-orthogonal modes in lossless multimode cavities," *IEEE J. Quantum Electron.*, vol. 40, no. 10, pp. 1511–1518, Oct. 2004.
- [27] S. Fan, W. Suh, and J. D. Joannopoulos, "Temporal coupled-mode theory for the Fano resonance in optical resonators," *J. Opt. Soc. Amer. A, Opt. Image Sci. Vis.*, vol. 20, no. 3, pp. 569–572, Mar. 2003.
- [28] Z. Xu, K. Song, and P. Mazumder, "Spoofed surface plasmon polariton (SSPP) gap structure for high sensitivity bio-sensing in THz," in *Proc. IEEE Conf. Nanotechnol.*, Beijing, China, Aug. 2013, pp. 311–314.



**Mahdi Aghadjani** received the B.S. degree in electrical engineering from the Iran University of Science and Technology, Tehran, Iran, and the M.S. degree in electrical engineering from the University of Tehran, Tehran. He is currently pursuing the Ph.D. degree with the Department of Electrical Engineering and Computer Science, University of Michigan, Ann Arbor, MI, USA.

His current research interests include designing optical and terahertz devices.



**Pinaki Mazumder** (S'84–M'87–SM'95–F'99) received the Ph.D. degree from the University of Illinois at Urbana-Champaign, Urbana, IL, USA, in 1988.

He is currently a Professor with the Department of Electrical Engineering and Computer Science, University of Michigan, Ann Arbor, MI, USA.

Dr. Mazumder is a fellow of the American Association for the Advancement of Science in 2008.